ARTICLE

Check for updates

# TRPV1$^+$ sensory nerves modulate corneal inflammation after epithelial abrasion via RAMP1 and SSTR5 signaling

Jun Liu[1,2,4], Shuoya Huang[1,2,4], Ruoxun Yu[1,2], Xinwei Chen[1,2], Fanying Li[1,3], Xin Sun[1,2], Pengyang Xu[1], Yijia Huang[1,2], Yunxia Xue[1], Ting Fu[1] and Zhijie Li[1,2]✉



Timely initiation and termination of inflammatory response after corneal epithelial abrasion is critical for the recovery of vision. The cornea is innervated with rich sensory nerves with highly dense TRPV1 nociceptors. However, the roles of TRPV1$^+$ sensory neurons in corneal inflammation after epithelial abrasion are not completely understood. Here, we found that depletion of TRPV1$^+$ sensory nerves using resiniferatoxin (RTX) and blockade of TRPV1 using AMG-517 delayed corneal wound closure and enhanced the infiltration of neutrophils and γδ T cells to the wounded cornea after epithelial abrasion. Furthermore, depletion of TRPV1$^+$ sensory nerves increased the number and TNF-α production of corneal CCR2$^+$ macrophages and decreased the number of corneal CCR2$^-$ macrophages and IL-10 production. In addition, the TRPV1$^+$ sensory nerves inhibited the recruitment of neutrophils and γδ T cells to the cornea via RAMP1 and SSTR5 signaling, decreased the responses of CCR2$^+$ macrophages via RAMP1 signaling, and increased the responses of CCR2$^-$ macrophages via SSTR5 signaling. Collectively, our results suggest that the TRPV1$^+$ sensory nerves suppress inflammation to support corneal wound healing via RAMP1 and SSTR5 signaling, revealing potential approaches for improving defective corneal wound healing in patients with sensory neuropathy.

*Mucosal Immunology* (2022) 15:867–881; https://doi.org/10.1038/s41385-022-00533-8

## INTRODUCTION

The cornea, a transparent and avascular tissue in the anterior segment of the eyeball, provides almost 70% refraction of the optical axis[1,2]. Owing to external exposure, the cornea is susceptible to mechanical or chemical injury[3,4]. Modern laser refractive surgery further amplifies this problem[5,6]. The risk of microbial infections, keratohelcosis, and stromal turbidity increases if the wounded cornea does not completely heal in time[7]. Therefore, completely understanding the mechanisms of corneal wound healing and identifying more potential targets for the therapy of defective wound healing in the cornea are critical.

Healing of the injured cornea is a complicated process, which involves re-epithelialization, inflammation, and cell proliferation at the early stage and corneal stromal remodeling at the late stage[1]. Among these events, balanced inflammation is crucial for high-quality healing[8–13]. Immune cells involved in corneal wound repair play a distinct role in the wound healing process. After corneal injury, neutrophils are the first to migrate to the injured cornea from corneal limbal vessels as the first-line immune cells[8]. Infiltrating neutrophils clean the wound area by releasing enzymes and phagocytosing and promote the ingrowth of corneal nerves by releasing growth factors such as vascular endothelium growth factor[9]. Resident and infiltrating γδ T cells in the injured cornea recruit neutrophils to the inured cornea by producing IL-17A and directly stimulate the division and migration of corneal epithelial cells by producing IL-22[14]. Two different macrophage subsets (CCR2$^+$ and CCR2$^-$) stimulate inflammatory responses by releasing pro-inflammatory cytokines and inhibit the inflammatory response by producing immunosuppressive cytokines, respectively[12]. Infiltrating natural killer cells prevent the excessive accumulation and tissue-injuring activity of neutrophils after corneal injury[11]. The resident innate lymphoid type 2 cells in the corneal limbus promote corneal epithelial division and migration by producing amphiregulin, a type of epidermal growth factor[15]. Any event that disturbs the migration and activity of these immune cells affects the quality of corneal wound healing.

The cornea is densely innervated by three main functional classes of sensory neurons, broadly classified as polymodal nociceptors, pure mechano-nociceptors, and cold-sensing neurons[16,17]. After sensing different stimuli, such as mechanical, chemical, or thermal stimuli, these receptors initiate essential protective reflexes, such as increased blinking rate and tear secretion[18,19]. Thus, these sensory fibers play a crucial role in the maintenance of corneal homeostasis and the response to different stimulations. The transient receptor potential vanilloid 1 (TRPV1) positive nerve fibers comprise approximately 45% of the sensory nerves[20]. Recently, TRPV1 has been extensively studied for its use in the regulation of inflammation[21–24]. Activation of TRPV1$^+$ sensory nerves can exert pro- and anti-inflammatory effects in vivo, depending on the type of neuropeptide released. For example, these nerve fibers have been shown to inhibit the recruitment of neutrophils and γδ T cells in bacterially infected

[1]International Ocular Surface Research Center, Institute of Ophthalmology, and Key Laboratory for Regenerative Medicine, Jinan University, Guangzhou, China. [2]Department of Ophthalmology, The First Affiliated Hospital of Jinan University, Guangzhou, China. [3]Department of Microbiology and Immunology, School of Medicine, Jinan University, Guangzhou, China. [4]These authors contributed equally: Jun Liu, Shuoya Huang. ✉email: tzhijieli@jnu.edu.cn

Received: 4 September 2021 Revised: 25 April 2022 Accepted: 24 May 2022
Published online: 9 June 2022

lung tissue by secreting calcitonin gene-related peptide (CGRP)[25] to increase IL-10 expression and reduce TNF-α expression in macrophages[26,27]. However, following lung injury, released substance P (SP) has been shown to stimulate IL-6, TNF-α, and MCP-1 production in lung epithelial cells[28], while secreted SST suppresses the systemic immune responses[29,30]. In the *Pseudomonas aeruginosa* keratitis model, sensory nerves alter corneal inflammation progress through a CGRP-driven increase in neutrophil recruitment to the site of infection but inhibit its bactericidal activity[31] and promote the transformation of macrophages from the M1 to M2 phenotype[32]. In the topical resiniferatoxin (RTX)-induced TRPV1$^+$ sensory nerve denervation model[33] and in the genetically TRPV1 deficient mouse model[34], a significant delay in corneal wound repair was found. However, this delay was significantly reversed by topical application of neuropeptides CGRP, substance P (SP), and vasoactive intestinal peptide (VIP)[33]. Despite this knowledge, the underlying mechanisms of TRPV1 in mediating the post-traumatic corneal inflammatory response have not been well defined.

Considering the important role of the TRPV1$^+$ sensory nerves in systemic and local inflammation, we hypothesized that TRPV1$^+$ sensory nerves in the cornea might also play an important role in the corneal wound healing process. To address this issue, we investigated wound closure and inflammatory reaction after corneal abrasion in mice with RTX-mediated ablation of TRPV1$^+$ sensory nerves and AMG-517-mediated pharmacological blockade of TRPV1. Furthermore, we analyzed the transcriptional profiles for neuropeptide receptors in neutrophils, γδ T cells, and macrophages, which are involved in inflammation in the wounded cornea. With topical administration of the agonists or antagonists for these neuropeptide receptors, we further validated the importance of the related signaling pathway in modulating inflammation after corneal epithelial abrasion. Overall, our findings reveal a previously unexpected, but critical, mechanistic role for TRPV1$^+$ sensory nerves coordinating corneal inflammation after epithelial abrasion via neuropeptide receptors.

## RESULTS

### Ablation of TRPV1$^+$ sensory nerves impaired corneal wound closure

Immunostaining of cornea showed that corneal nerve terminal expressed TRPV1 (Fig. 1a). To determine the role of TRPV1$^+$ sensory nerves in corneal wound healing, RTX was used to deplete TRPV1$^+$ sensory nerves as described previously[35,36]. As expected, after subcutaneous injection with RTX for four weeks, both the expression of TRPV1 (Fig. 1b, d), the density of nerve fibers in the cornea (Fig. 1e, f, g) and the corneal sensitivity (Fig. 1h) decreased significantly. Compared with in vehicle-treated animals, wound closure (Fig. 1i) and epithelial division (Fig. 1k, l) were significantly impaired following corneal abrasion in RTX-treated animals. To investigate the alteration in the molecular signature between the RTX-treated and vehicle-treated corneas after corneal abrasion, the transcriptomic profiles were determined using RNA sequencing. The expression of genes involved in the metabolic process and the cell proliferation and migration decreased in RTX-treated mice (Fig. 2a, b). Furthermore, Cytoscape network analysis of corneal gene transcription revealed that genes involved in epithelial cell proliferation and migration were mostly down-regulated, whereas those involved in the epithelial cell apoptosis were mostly up-regulated (Fig. 2c). Thus, the changes in corneal gene transcription indicated that RTX treatment delayed corneal wound healing.

### Ablation of TRPV1$^+$ sensory nerves increased inflammation after epithelial abrasion

To determine the influence of TRPV1$^+$ sensory nerves on corneal inflammation after epithelial abrasion, we first analyzed the alteration in corneal genes involved in immune response. Data showed that the expression of genes involved in immunity and chemotaxis, especially those of *Il6*, *Tnf*, *Cxcr1*, and *Cxcr2*, increased in the corneas of RTX-treated mice (Fig. 3a). Cytoscape network analysis revealed that genes involved in the neutrophil chemotaxis, migration, activation, degranulation, mediated cytotoxicity, and the γδ T cell activation and differentiation were mostly up-regulated (Fig. 3b). Next, we investigated the influx of neutrophils and γδ T cells in the injured cornea. Immunostaining of the cornea showed that the number of infiltrating neutrophils within the region of the corneal wound margin at 6, 12, 18, 24, 30, and 36 h after epithelial abrasion and that of infiltrating γδ T cells at 24, 30, and 36 h after epithelial abrasion in RTX-treated mice were significantly higher than those in vehicle-treated mice (Fig. 3d, e). Flow cytometric analysis at 18 h after corneal abrasion further showed that ablation of TRPV1$^+$ sensory nerves exacerbated corneal inflammation after corneal injury (Fig. 3g). These data suggest that RTX treatment exacerbated corneal inflammation after epithelial abrasion.

### Blockade of TRPV1 function impaired corneal wound closure and exaggerated inflammation after epithelial abrasion

To further confirm the specific roles of TRPV1$^+$ sensory nerves in modulating corneal wound healing and inflammation after epithelial abrasion, we topically applied AMG-517, a TRPV1 antagonist[37,38], and inhibited the function of TRPV1$^+$ sensory nerves. Consistent with the results of our previous studies, the wound in control mice closed 24 h after epithelial abrasion. However, corneal wounds in AMG-517-treated mice did not close until 30 h after epithelial abrasion (Fig. 4a). Similarly, the number of dividing epithelial cells in AMG-517-treated corneas was significantly lower than in vehicle-treated corneas (Fig. 4b). To evaluate the effects of blockade of TRPV1 function on injury-induced inflammation after abrasion, the number of infiltrating neutrophils and γδ T cells in the cornea was enumerated in vehicle-treated and AMG-517-treated corneas. After treatment with AMG-517, the number of neutrophils within the region of the corneal wound margin and γδ T cells within the perilimbal region significantly increased at 12, 18, 24, and 30 h after epithelial abrasion (Fig. 4c). In addition, flow cytometric analysis further confirmed that the number of neutrophils and γδ T cells in AMG-517-treated cornea was more than in the cornea of vehicle-treated mice at 18 h after epithelial abrasion (Fig. 4d).

### TRPV1$^+$ sensory nerves suppressed the recruitment of neutrophils and γδ T cells via RAMP1 and SSTR5 signals

Sensory nerves modulate the responses of immune cells, usually by releasing neuropeptides[23,24]. Immunostaining of cornea showed that nerve fibers expressed CGRP and SST (Fig. 5a). To determine whether the RTX-mediated ablation of TRPV1$^+$ sensory nerves affected the production of neuropeptides in the cornea, we compared the gene expression of neuropeptides in corneal cells using quantitative polymerase chain reaction (qPCR) analysis, as mRNA localization and local protein synthesis in axons have been reported previously[39,40]. Both *Cgrp* and *Sst* levels decreased after RTX treatment 12 h post-epithelial abrasion (Fig. 5b). Neutrophils in the cornea expressed the CGRP receptor gene, *Ramp1*, and the SST receptor genes, *Sstr1-5*. Among these, *Sstr5* was predominately expressed in neutrophils. However, the γδ T cells in the cornea expressed *Ramp1* and *Sstr5* (Fig. 5c). This suggests that the increase in the recruitment of neutrophils and γδ T cells to the RTX-treated cornea may be due to the decrease in the activity of RAMP1-CGRP or SST-SSTR5 signaling in the cornea. To confirm this hypothesis, we first block the function of RAMP1 and SSTR5 and observed the alteration of neutrophils and γδ T cells. When the injured corneas of normal mice were topically treated with BIBN 4096, the RAMP1 antagonist, and BIM 23056, the SSTR5 antagonist, the number of both neutrophils and γδ T cells in the

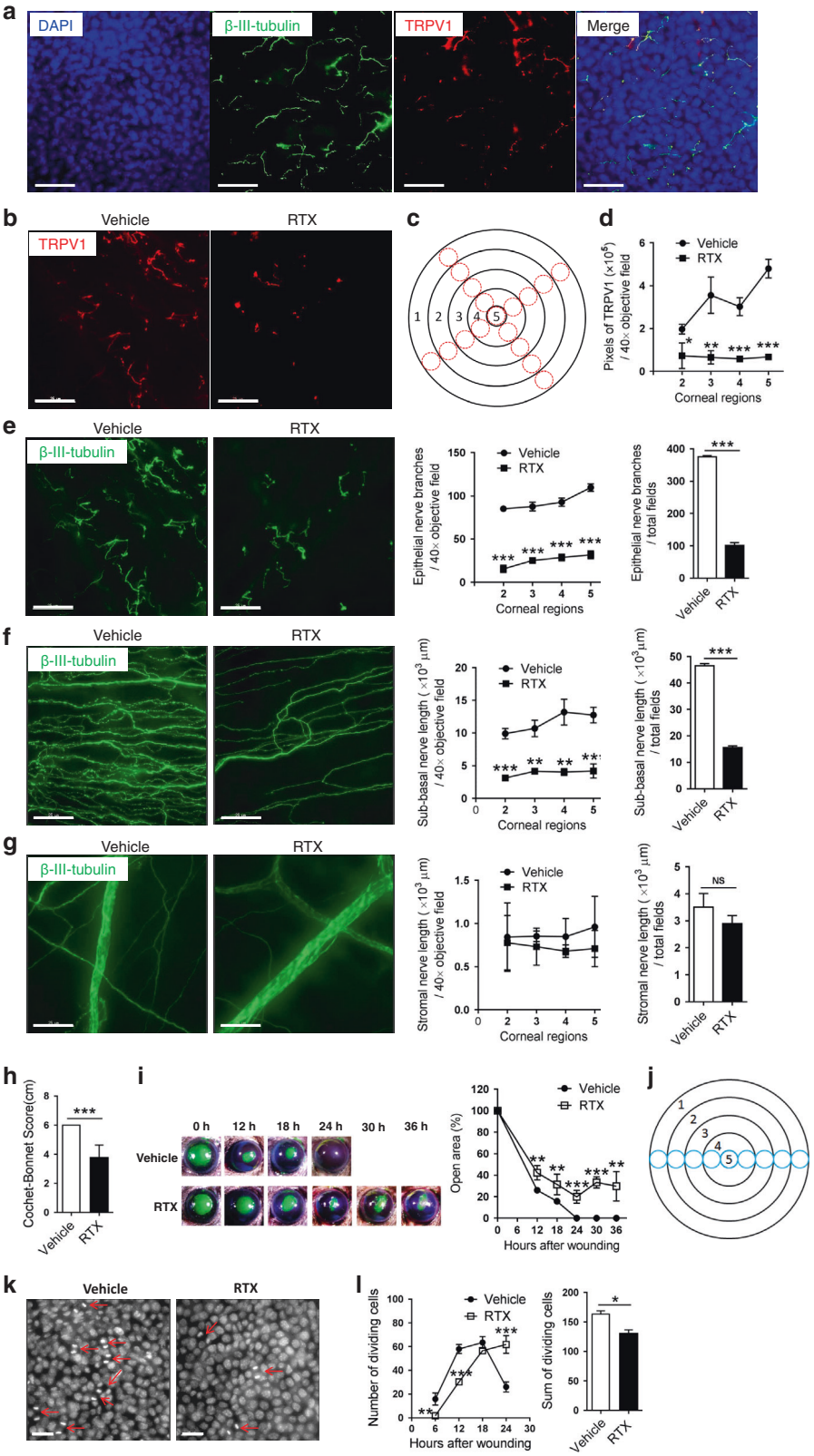


cornea increased (Fig. 5d, e). Second, eyedrops of CGRP or L-817818, an SSTR5 agonist, were administered to the eyes of the RTX-treated mice. The results showed that the number of neutrophils and γδ T cells (Fig. 5f, g), the expression of *Il1β* and *Il18* in neutrophils (Fig. 5h), and the expression of *Il17a* and *Tnfα* in γδ T cells (Fig. 5i) in the cornea of RTX-treated mice decreased after treatment with CGRP or L-817818. Thus, these results revealed that the TRPV1$^{+}$ sensory nerves inhibited the infiltration

**Fig. 1 Effects of resiniferatoxin (RTX) treatment on corneal wound healing. a** Immunostaining of epithelial nerve branches with anti-β-III tubulin antibody conjugated with Alexa Fluor 488 and TRPV1 with anti-TRPV1 antibody (Scale bars = 25 μm). **b** Immunostaining of TRPV1 with anti-TRPV1 antibody in corneas of vehicle-treated and RTX-treated mice (Scale bars = 25 μm). **c** A schematic view of counting the pixels of TRPV1, the nerve branches, and the nerve length in cornea. Cornea with complete limbus can be divided into five zones (1–5) from limbus to central cornea. Region 1 is in the limbus, and regions 2–5 are in the cornea. The average of pixels of TRPV1, nerve branches, or nerve length in four fields within the each region counted under the 40× objective. **d** Comparison of the expression of TRPV1 (represented as pixels) in each corneal region between vehicle-treated and RTX-treated mice ($n = 6$ mice per group). **e**–**g** Comparison of epithelial nerve branches, sub-basal nerve length, and stromal nerve length in each corneal region between vehicle-treated and RTX-treated mice ($n = 6$ mice per group). Left images show the staining of epithelial nerve branches, sub-basal nerve and stromal nerve fibers in cornea of vehicle-treated and RTX-treated mice (Scale bars = 25 μm). **h** Analysis of corneal sensitivity in vehicle-treated and RTX-treated mice ($n = 6$ mice per group). **i** Observation of wound closure in the cornea of vehicle-treated and RTX-treated mice. Images on the left show the staining of the wounded corneal area at each time point after epithelial abrasion with fluorescein sodium. The graph on the right shows the dynamic changes in the ratio of wounded corneal area within the whole corneal area in vehicle-treated and RTX-treated mice ($n = 6$ mice per group). **j** A schematic view of counting dividing epithelial cells in the cornea. Dividing epithelial basal cells were counted in nine microscopic fields across the cornea from limbus to limbus; fields were observed under a 40× objective lens, and the total dividing cell number from the nine microscopic fields, was used as the indicator of dividing cell number of corneal epithelia. **k** 4′,6-Diamidino-2-phenylindole staining of epithelial basal cells in the cornea of vehicle-treated and RTX-treated mice under a 40× objective field (scale bars = 25 μm). The red arrows marking coupled cell nuclei represent the dividing epithelial cells. **l** Comparison of the number of dividing epithelial cells in the cornea between vehicle-treated mice and RTX-treated mice at each time point after wounding (left graph) and from all time points (right graph) ($n = 6$ mice per group at each time point). Data are presented as mean ± SD. $^{*}P < 0.05$, $^{**}P < 0.01$, and $^{***}P < 0.001$.

of neutrophils and γδ T cells to the cornea and the expression of pro-inflammatory cytokines in neutrophils and γδ T cells via RAMP1 and SSTR5 signaling.

### TRPV1$^+$ sensory nerves regulated the responses of CCR2$^-$ and CCR2$^+$ corneal macrophages after epithelial abrasion via RAMP1 and SSTR5 signals

Macrophages modulate various types of inflammatory response and are controlled by sensory nerves[41,42]. Hence, we speculated that corneal macrophages may be regulated by TRPV1$^+$ sensory nerves during corneal wound healing. Our previous study showed that corneal macrophages can be classified into CCR2$^+$ and CCR2$^-$ subsets. The CCR2$^+$ macrophages (M1 subtype) promoted inflammation in the injured cornea with secretion of TNF-α and IL-1β, whereas the CCR2$^-$ macrophages (M2 subtype) inhibited inflammation with the secretion of IL-10[12]. In this study, Cytoscape network analysis of corneal gene transcription showed that genes involved in monocyte chemotaxis and macrophage differentiation in RTX-treated-corneas were mostly up-regulated. In the gene set related to macrophage activation, we found that the expression of M1 macrophage-related genes (*Cd86*, *Cd80*, *Fpr2*, and *Tnf*)[43–45] increased, whereas the expression of M2 macrophage-related genes (*Cxcl13*, *Sucnr1*, *Cd163*, and *Retnla*)[45–48] decreased (Fig. 6a). Flow cytometric analysis showed that in the cornea of RTX-treated mice, the number of CCR2$^+$ macrophages increased, and that of CCR2$^-$ macrophages decreased at 21 h after epithelial abrasion (Fig. 6e). In addition, the production of TNF-α in CCR2$^+$ macrophages increased, and that of IL-10 in CCR2$^-$ macrophages decreased after RTX treatment 21 h post-epithelial abrasion (Fig. 6f). Using flow cytometric sorting and qPCR analysis, we found that corneal CCR2$^+$ and CCR2$^-$ macrophages expressed *Ramp1* and *Sstr1–5*. Among these, *Ramp1* was predominantly expressed in CCR2$^+$ macrophages, and *Sstr5* in CCR2$^-$ macrophages (Fig. 6g). To investigate the roles of RAMP1 and SSTR5 in regulating the responses of corneal macrophages, we treated injured corneas of normal mice with drops of BIBN 4096, a RAMP1 antagonist, or BIM 23056, an SSTR5 antagonist. The number of CCR2$^+$ macrophages increased, whereas that of the CCR2$^-$ macrophages did not change considerably after BIBN 4096 treatment (Fig. 6h). In contrast, the number of CCR2$^-$ macrophages decreased, whereas that of CCR2$^+$ macrophages did not change significantly after BIM 23056 treatment (Fig. 6i). In addition, the production of TNF-α in CCR2$^+$ macrophages increased after BIBN 4096 treatment and that of IL-10 in CCR2$^-$ macrophages decreased after BIM 23056 treatment (Fig. 6j). Furthermore, the number of CCR2$^+$ macrophages in the cornea and the production of TNF-α in these cells from RTX-treated mice decreased after using CGRP locally (Fig. 6k). The number of CCR2$^-$ macrophages in the cornea and the amount of IL-10 produced by these cells from RTX-treated mice can be increased with local application of L-817818 (Fig. 6l). Therefore, TRPV1$^+$ sensory nerves suppress the response of CCR2$^+$ macrophages via RAMP1 signaling and promote the response of CCR2$^-$ macrophages via SSTR5 signaling in the cornea.

### CGRP and L-817,818 promoted corneal wound healing in RTX-treated mice

Both CGRP and L-817,818 can decrease the inflammation after RTX-mediated depletion of TRPV1$^+$ sensory nerves. To investigate whether CGRP and L-817,818 promoted the healing of injured corneas in RTX-treated mice, drops of CGRP and L-817,818 were individually administered to these mice. The wound size of corneas in RTX-treated mice decreased after treatment with CGRP (Fig. 7a) or L-817,818 (Fig. 7c) 12, 18, and 24 h after epithelial abrasion. The number of dividing epithelial cells in RTX-treated mice significantly increased after treatment with CGRP (Fig. 7b) or L-817,818 (Fig. 7d) 18 h after epithelial abrasion. This indicated that activation of RAMP1 and SSTR5 can reverse the effect of RTX on corneal wound healing.

## DISCUSSION

In this study, we confirmed that the TRPV1$^+$ sensory nerves are closely involved in the wound repair process of the cornea by balancing the inflammatory response, mainly via the RAMP1 and SSTR5 signals. We observed that (1) both ablation of TRPV1$^+$ sensory nerves and blockade of TRPV1 increased inflammation in the cornea after epithelial abrasion; (2) activation of both RAMP1 and SSTR5 reduced the accumulation and pro-inflammatory cytokine expression of neutrophils and γδ T cells in the cornea of TRPV1$^+$ sensory nerve-ablated mice; (3) activation of RAMP1 reduced the CCR2$^+$ macrophage distribution in the cornea and TNF-α expression, whereas activation of SSTR5 increased the CCR2$^-$ macrophage distribution in the cornea and IL-10 expression. These events act together to limit the excessive inflammatory response after corneal injury and promote the wound repair process in the cornea. Finally, we confirmed that topical administration of both CGRP and SSTR5 agonists improved the impaired corneal wound healing in the TRPV1$^+$ sensory nerve-ablated mice. The data obtained in this study further support the uniqueness of the cornea as an immune-privileged tissue and its corresponding mechanisms.

TRPV1$^+$ sensory nerves in the cornea play a key role in maintaining corneal homeostasis and responding to different

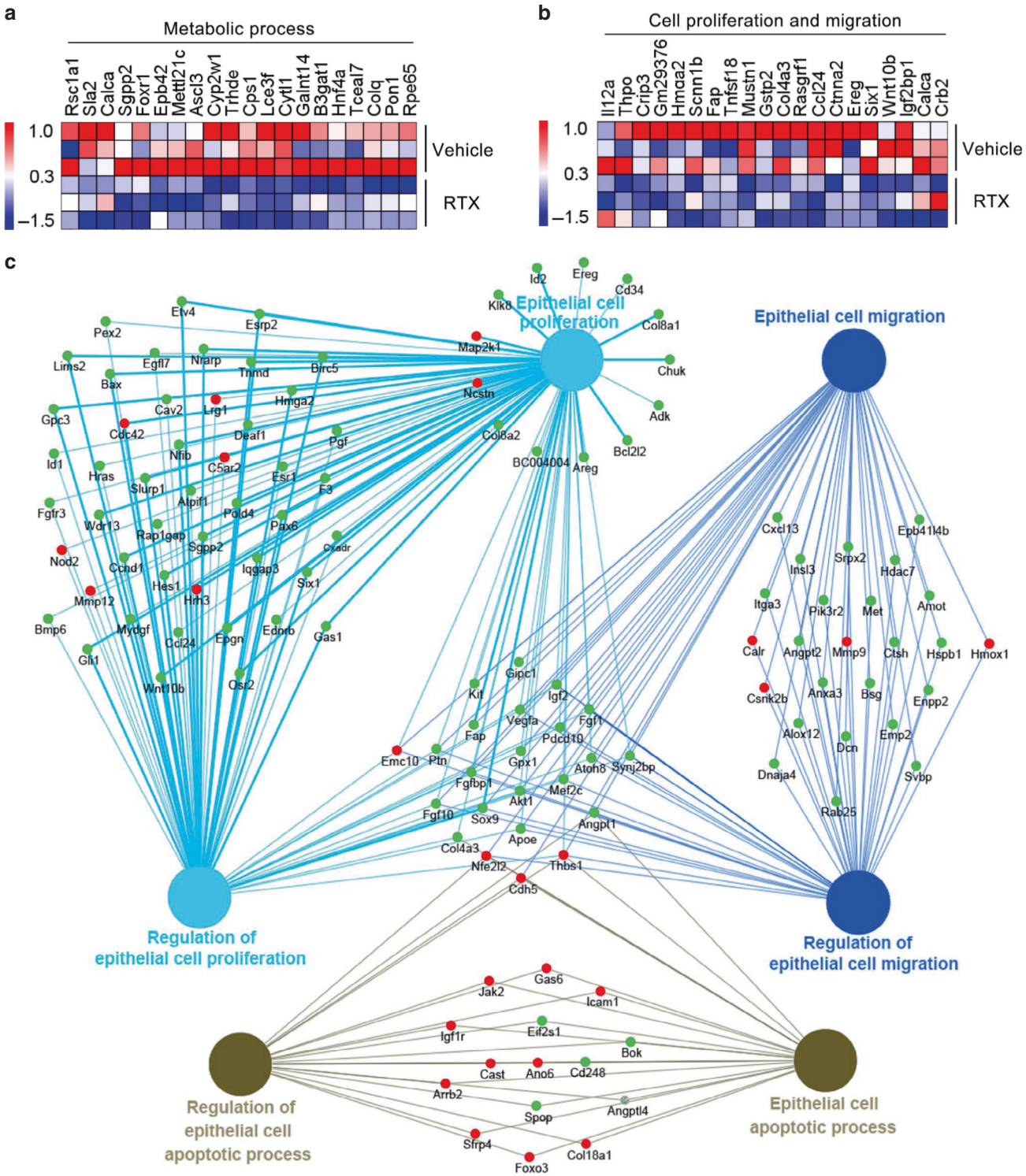


**Fig. 2 Effects of resiniferatoxin (RTX) treatment on transcriptomic profiles of wounded corneas. a**, **b** Heat maps show the expression of genes involved in the metabolic process and the cell proliferation and migration in cornea of vehicle-treated mice and RTX-treated mice ($n = 3$ independent experiments, 3 mice per experiment in each group). **c** Cytoscape network analysis of transcripts involved in the epithelial cell proliferation, migration, and apoptosis, and the regulation of epithelial cell proliferation, migration, and apoptosis (up-regulated genes are shown in red and down-regulated genes are shown in green).

external stimuli[16–19]. In the present study, a comparative analysis of the corneal wound repair process and transcriptome after chemical TRPV1$^+$ sensory nerve ablation and pharmacological intervention in TRPV1 signaling confirmed that the presence of TRPV1$^+$ sensory nerves coordinated the re-epithelialization process after corneal epithelial abrasion, including epithelial division and migration. These results are consistent with previous findings in the corneas of TRPV1 genetically deficient and chemically TRPV1-ablated mice[33,34]. Similarly, the present study also found that chemical ablation of TRPV1$^+$ nerves or

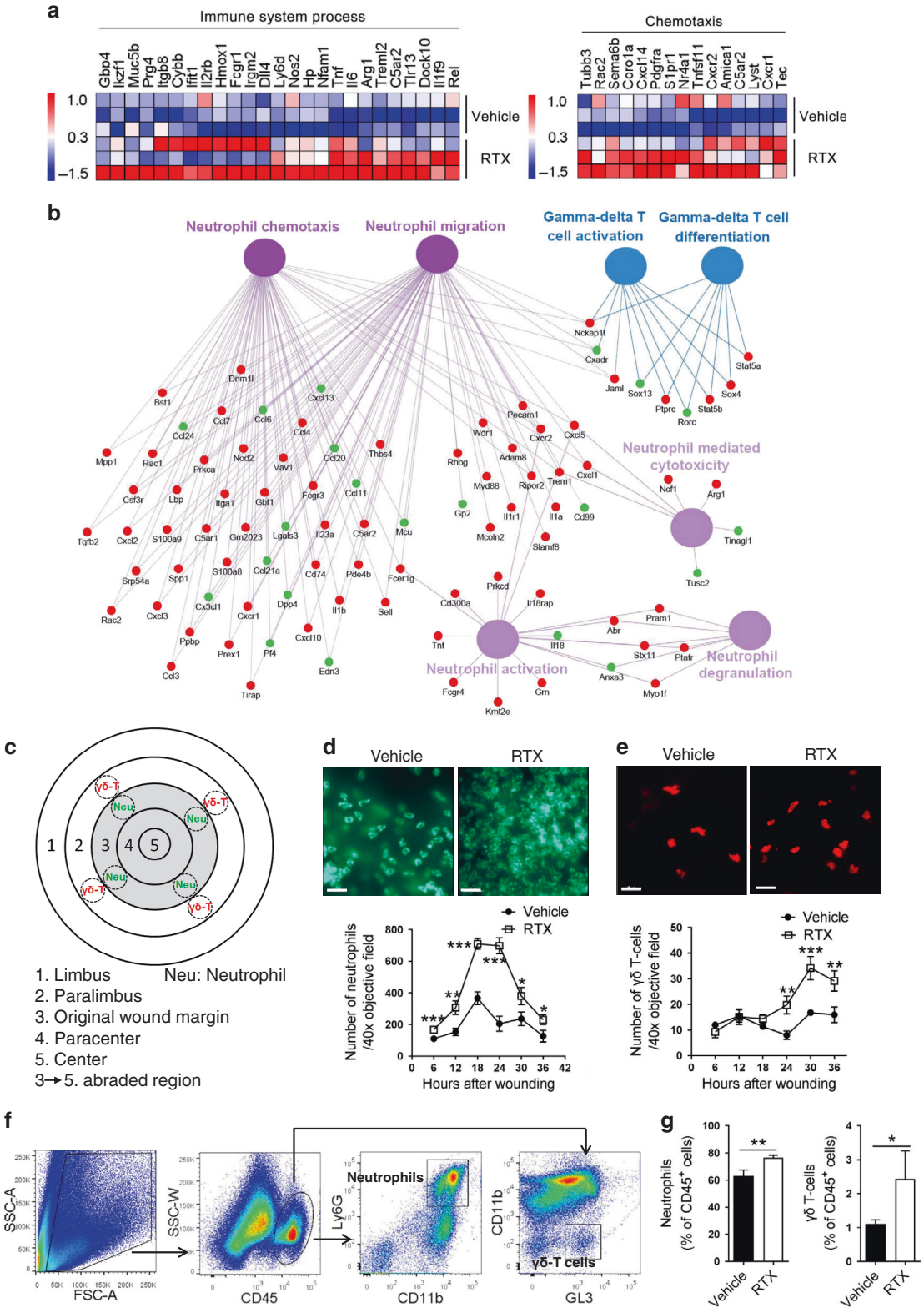


pharmacological blockade of the TRPV1 signaling pathway significantly affected the extent of the inflammatory response following corneal injury, mainly in the form of increased recruitment of inflammatory cells (neutrophils, γδ T cells and CCR2$^{+}$ macrophages) to the injured cornea and the expression of pro-inflammatory cytokine transcripts in the cornea. This is coherent with findings from other barrier site models of inflammation, such as pulmonary and cutaneous *S. aureus* infection[25,49]. Overall, these results suggest that TRPV1$^{+}$ sensory nerves in the cornea play an important regulatory role, both qualitative and quantitative, in wound repair after corneal abrasions. Therefore, it is important to further explore the

**Fig. 3 Effects of ablation of TRPV1$^+$ sensory nerves on corneal inflammation after epithelial abrasion. a** Heat maps show the expression of genes involved in the immune system processes and the chemotaxis in corneas of vehicle-treated mice and resiniferatoxin (RTX)-treated mice ($n = 3$ independent experiments, 3 mice per experiment in each group). **b** Cytoscape network analysis of transcripts involved in the neutrophil chemotaxis, migration, activation, degranulation, and mediated cytotoxicity, and the γδ T cell activation and differentiation (up-regulated genes are shown in red and down-regulated genes are shown in green). **c** A schematic view of counting neutrophils and γδ T cells in the cornea. The average number of neutrophils or γδ T cells in four fields counted under the 40× objective. **d** Alteration in neutrophil number in the cornea after RTX treatment analyzed using whole-mount immunostaining of the cornea. The upper two images show the corneal immunostaining using anti-mouse Ly6G antibody conjugated with fluorescein isothiocyanate under the 40× objective field (scale bars = 25 μm). The lower graph shows the dynamic changes in neutrophil number in vehicle-treated mice and RTX-treated mice after epithelial abrasion ($n = 6$ mice per group at each time point). **e** Changes in the γδ T cell number in the cornea after RTX treatment were analyzed using whole-mount immunostaining of the cornea. The upper two images show the immunostaining of the cornea using anti-GL3 antibody conjugated with phycoerythrin (PE) under the 40× objective field (scale bars = 25 μm). The lower graph shows the dynamic changes in γδ T cell number in vehicle-treated mice and RTX-treated mice after epithelial abrasion ($n = 6$ mice per group at each time point). The method for counting γδ T cells is identical to that used for neutrophil counting. **f** The gating strategy of flow cytometry for analyzing neutrophils and γδ T cells. **g** Comparison of neutrophils and γδ T cells in the cornea between vehicle-treated mice and RTX-treated mice 18 h after epithelial abrasion by using flow cytometric analysis ($n = 3$ independent experiments, 5 mice per experiment in each group). Data are presented as mean ± SD. $^*P < 0.05$, $^{**}P < 0.01$, and $^{***}P < 0.001$.

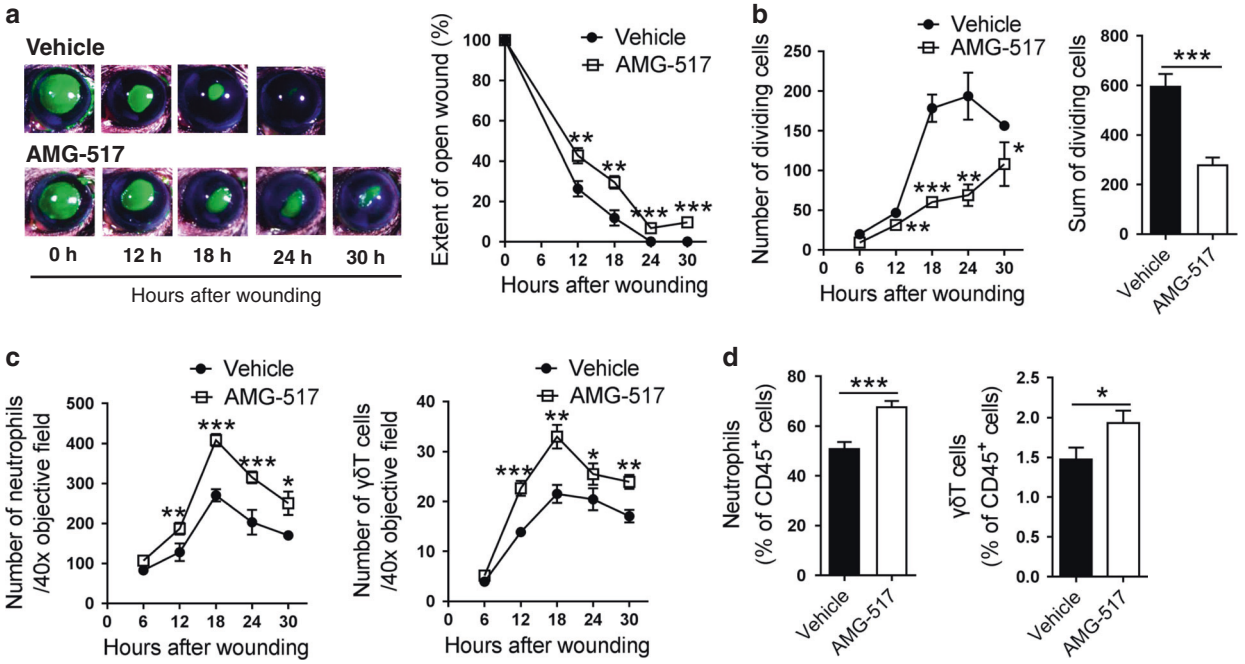


**Fig. 4 Influence of TRPV1 blockade on corneal wound healing and inflammation after epithelial abrasion. a** Observation of corneal wound closure in vehicle-treated mice and AMG-517 treated mice. Images on the left show the staining of corneal wounds at each time point after epithelial abrasion with fluorescein sodium. The graph on the right shows the dynamic changes in the ratio of wounded area within the whole corneal area of vehicle-treated mice and AMG-517 treated mice ($n = 6$ mice per group). **b** Comparison of the number of dividing epithelial cells at each time point (*left*) and at all time points (*right*) after epithelial abrasion in vehicle-treated mice and AMG-517 treated mice ($n = 6$ mice per group at each time point). **c** Analysis of the difference in the number of neutrophils (*left*) and γδ T cells (*right*) in the cornea of vehicle-treated mice and AMG-517 treated mice at each time point after epithelial abrasion using immunostaining of corneal whole-mount ($n = 6$ mice per group at each time point). **d** Comparison of the number of neutrophils (*left*, $n = 3$ independent experiments, 5 mice per experiment in each group) and γδ T cells (*right*, $n = 3$ independent experiments, 5 mice per experiment in each group) in the cornea of vehicle-treated mice and AMG-517 treated mice at 18 h after epithelial abrasion using flow cytometric analysis. Data are presented as mean ± SD. $^*P < 0.05$, $^{**}P < 0.01$, and $^{***}P < 0.001$.

underlying molecular mechanisms, particularly in the inflammatory response.

Neutrophils are the first line of inflammatory cells recruited to the wounded cornea after corneal injury[8,50,51]. These cells contribute to its repair process by producing certain growth factors, such as VEGF, besides their role in killing contaminating microbes and cleaning the wound through the secretion of certain enzymes[8,50,52]. To explore the underlying mechanisms by which TRPV1$^+$ nerves regulate neutrophil migration and function following corneal wounding, we first demonstrated that neutrophils trafficking to the injured cornea express the receptor SSTR5 corresponding to the neuropeptide SST. Second, topical administration of SSTR5 agonists reversed the increase in neutrophil infiltration induced by TRPV1$^+$ nerve ablation of the cornea. However, neutrophil recruitment to the site of infection in both pulmonary and cutaneous models of infection is mainly via sensory neuropeptide CGRP receptor RAMP1-mediated signaling[25,49] The reason for this discrepancy may be due to differences in the type, origin, and function of sensory nerve fibers at different barrier sites[53–55] or different local microenvironments[56,57].

Several studies have shown a close association between TRPV1$^+$ neurons and γδ T cells at the barrier site[25,54,58–60]. When skin TRPV1$^+$ neurons are stimulated by the TLR7 agonist imiquimod, they promote IL-23 production by dermal dendritic cells, which in turn stimulates dermal γδ T cells to secrete IL-17A, IL-17F, and IL-22, ultimately leading to the recruitment of more neutrophils to

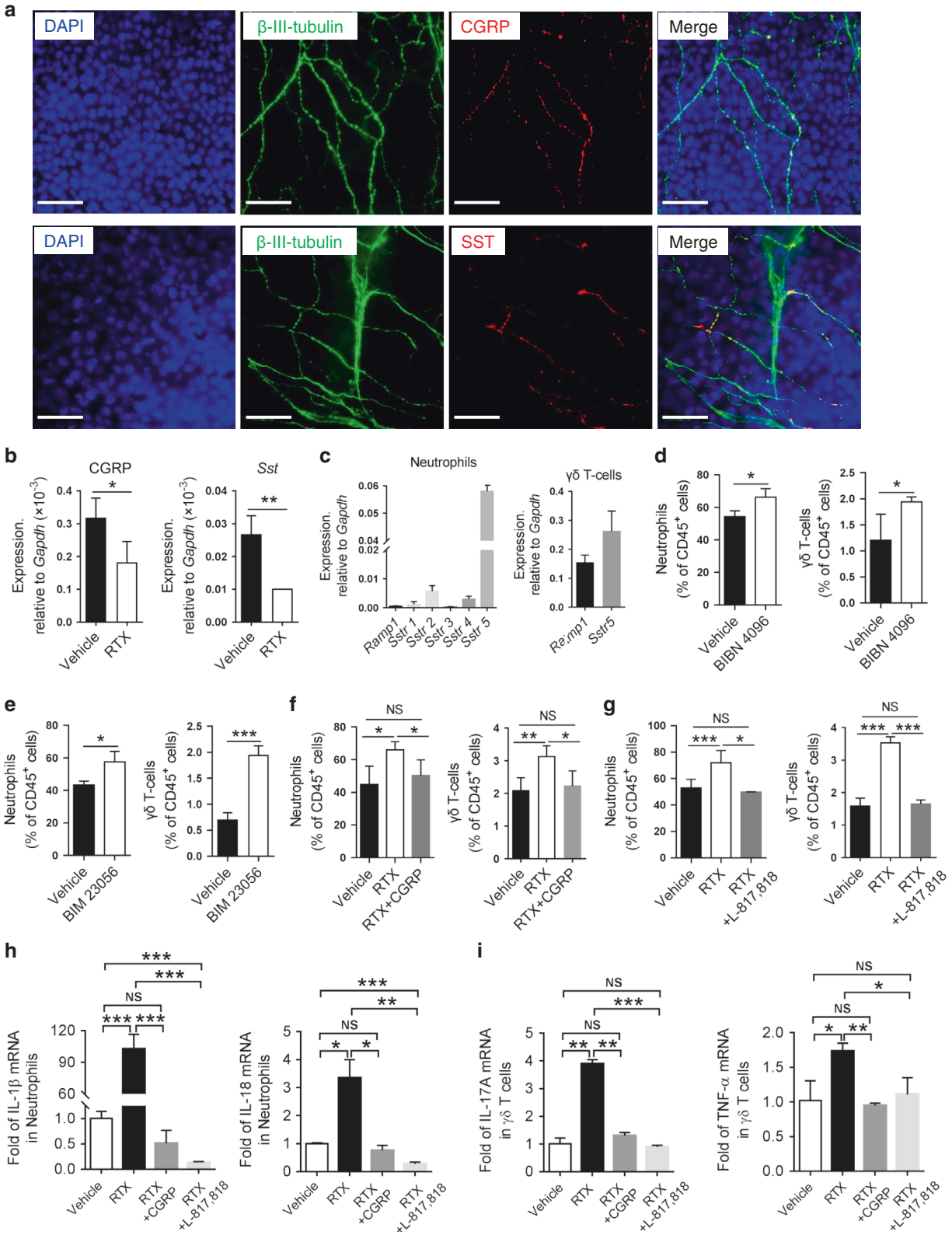


the skin and excessive keratinocyte proliferation[58,59]. Further studies have shown that cutaneous TRPV1$^+$ neurons are activated by *Candida albicans*-derived β-glucan to suppress *Candida albicans* infection by releasing CGRP to drive IL-23 production by dendritic cells to promote IL-17 production by cutaneous γδ T cells, thereby activating downstream pathways[60]. However, mouse models from lethal *S. aureus* pneumonia found that TRPV1$^+$ neurons down-regulated lung γδ T cells, leading to reduced recruitment of neutrophils, which are critical for bacterial clearance[25]. Removal of TRPV1$^+$ neuroreceptors by RTX in mice increased the number of γδ T cells in the lung and significantly improved their survival[25]. γδ T cells are also abundant on the

**Fig. 5 Analysis of the signaling of TRPV1$^+$ sensory nerves suppressing the responses of neutrophils and γδ T cells in the cornea.** **a** Immunostaining of nerve fibers with anti-β-III tubulin antibody conjugated with Alexa Fluor 488 and CGRP/SST with anti-CGRP/SST antibody in the cornea (scale bars = 25 μm). **b** Quantitative polymerase chain reaction (qPCR) analysis of the expression of *Cgrp* and *Sst* in the wounded cornea 12 h after the treatment with resiniferatoxin (RTX) ($n = 3$ independent experiments, 3 mice per experiment in each group). **c** qPCR analysis of the expression of *Ramp1* and *Sstr1–5* in the flow cytometry-sorted neutrophils and γδ T cells of the cornea ($n = 3$ independent experiments, 5 mice per experiment in each group). **d**, **e** Alteration in the number of neutrophils and γδ T cells in the cornea after treatment with BIBN 4096 or BIM 23056 ($n = 3$ independent experiments, 5 mice per experiment in each group). **f** Comparison of the number of neutrophils and γδ T cells in the cornea among vehicle-treated mice, RTX-treated mice, and RTX-treated mice treated with calcitonin gene-related peptide (CGRP) 18 h after epithelial abrasion ($n = 3$ independent experiments, 5 mice per experiment in each group). **g** Difference in the number of corneal neutrophils and γδ T cells among vehicle-treated mice, RTX-treated mice, and RTX-treated mice after treatment with L-817,818 18 h after epithelial abrasion ($n = 3$ independent experiments, 5 mice per experiment in each group). **h** Analysis of the expression of *Il1β* and *Il18* in the flow cytometry-sorted neutrophils from vehicle-treated mice, RTX-treated mice, RTX-treated mice treated with CGRP, and RTX-treated mice treated with L-817,818 ($n = 3$ independent experiments, 5 mice per experiment in each group). **i** Analysis of the expression of *Il17a* and *Tnfa* in the flow cytometry-sorted γδ T cells from vehicle-treated mice, RTX-treated mice, RTX-treated mice treated with CGRP, and RTX-treated mice treated with L-817,818 ($n = 3$ independent experiments, 5 mice per experiment in each group). Data are presented as mean ± SD. $^*P < 0.05$, $^{**}P < 0.01$, and $^{***}P < 0.001$.

ocular surface and play an important regulatory role in maintaining ocular surface homeostasis and in response to foreign stimuli[61]. Following corneal injury, γδ T cells that reside and emigrate into the injured cornea attract neutrophils and platelets, primarily through the production of IL-17A[9,14,62]. Both neutrophils and platelets have the potential to promote corneal nerve growth through the release of growth factors, such as VEGF[9,14,62]. This study explored the interaction between TRPV1 and γδ T cells in a corneal abrasion model through three parallel experiments. First, we found that γδ T cells recruited to the traumatized cornea continuously expressed the neuropeptide CGRP receptor RAMP1 and the SST receptor SSTR5. Second, injured corneas in mice following RTX removal of TRPV1$^+$ sensory nerves increased not only the number of locally recruited γδ T cells but also their expression of the pro-inflammatory cytokines *Tnfa* and *Il17a*. Consistent with this, local application of either CGRP or the SSTR5 agonist L-817,818 significantly reduced the number of γδ T cells recruited to injured corneas and their expression of the pro-inflammatory cytokines *Tnf* and *Il17a* in TRPV1$^+$ sensory nerve-ablated mice. Thus, consistent with the findings in the lungs[25], corneal stimulation of activated TRPV1$^+$ sensory nerves modulate the inflammatory response process after corneal trauma by altering the migration of γδ T cells and their cytokine expression through the release of the neuropeptides CGRP and SST.

Our previous study indicated that the balance between CCR2$^-$ and CCR2$^+$ macrophages regulated corneal inflammation via the autonomic nervous system during corneal wound healing[12,63]. Recent studies demonstrated that the macrophage reaction to different stimuli is also modulated by sensory nerve fibers via nociceptor-neuropeptide-macrophage interactions[64]. For instance, SP from sensory nerve fibers increased the number of M2 macrophages in arthritis[65]. CGRP up-regulated the expression of IL-10 in macrophages via cAMP/PKA signaling[66–68], whereas it inhibited the expression of TNF-α in the peritoneal macrophages[69]. Vasoactive intestinal peptide (VIP) decreased the expression of TNF-α and IL-6 in macrophages via cAMP-dependent signaling[70,71]. The neuropeptide TAFA4 released by the activation of Gαi-interacting protein$^+$ sensory neurons depresses the ultraviolet-induced skin inflammatory responses by promotion of embryonically derived TIM4$^+$ macrophages to produce IL-10[72]. Similarly, our data showed that TRPV1$^+$ nerve ablation with RTX significantly decreased the number of CCR2$^-$ macrophages and their expression of IL-10, whereas it increased the number of CCR2$^+$ macrophages and their expression of TNF-α. Further analysis confirmed that corneal CCR2$^+$ macrophages predominantly expressed the CGRP receptor *Ramp1*, whereas corneal CCR2$^-$ macrophages predominantly expressed *Sstr5*. Additionally, by topical administration of both agonist and antagonist for RAMP1 and SSTR5, respectively, we confirmed that the TRPV1$^+$ sensory nerves inhibited the CCR2$^+$ macrophage recruitment and TNF expression in the cornea via CGRP-RAMP1 signaling and promoted the production of IL-10 by CCR2$^-$ macrophages to dampen inflammation via SST-SSTR5 signaling. Thus, the integrated regulation of corneal macrophage responses by TRPV1$^+$ sensory nerves suppresses the inflammatory response after corneal injury.

Of note, other resident or infiltrating immune cells, such as natural killer cells[11], type 2 innate lymphoid cells (ILC2s)[15], dendritic cells[73,74], and mast cells[75–77], also coordinate the corneal wound healing process through unique functions and mechanisms. These cells also co-localize with TRPV1$^+$ sensory nerves and may express neuropeptide receptors for CGRP and SST. However, this study focused only on two subsets of macrophages, neutrophils, and γδ-T cells. Thus, the role of TRPV1$^+$ sensory nerves affecting other types of immune cells through the above neuropeptide receptors in coordinating the whole process of wound repair needs to be further clarified. In addition, TRPV1$^+$ sensory nerves also directly act on immune cells expressing corresponding receptors by releasing other neuropeptide mediators. Moreover, the TRPV1$^+$ sensory nerve plays a different regulatory role by releasing other neuropeptides directly binding to corresponding receptors expressed on immune cells. Studies have shown that SP from TRPV1$^+$ sensory nerves leads to degranulation of mast cells and the release of histamine and other cytokines by binding to Mas-related G protein-coupled receptor member B2 on mast cells[78], whereas VIP activates ILC2s[79] and type 2 T helper (Th2) cells through the VPAC2 receptor[80]. Finally, inflammatory mediators and even neuropeptides released from activated immune cells might sensitize TRPV1$^+$ sensory nerve fibers via a feedback way using gating of ion channels[23,81]. Therefore, the crosstalk between all these factors still needs to be explored spatially and temporally by more research.

Collectively, our results confirmed that TRPV1$^+$ sensory nerves suppressed corneal inflammation and promoted re-epithelialization after epithelial abrasion by inhibiting neutrophil and γδ T cell infiltration, inhibiting CCR2$^+$ macrophage response, and promoting CCR2$^-$ macrophage response via the RAMP1 and SSTR5 signaling pathways (Fig. 8). It is well known that corneal nerve density and corneal sensitivity are low in patients with diabetes. The corneas of these patients always show delayed wound healing and enhanced inflammation after injury. Our observations regarding the roles of TRPV1$^+$ sensory nerves in modulating corneal inflammation via RAMP1 and SSTR5 signaling may reveal potential targets for improving corneal wound healing in diabetics.

## MATERIALS AND METHODS

### Animals

C57BL/6 J mice without any eye diseases were purchased from the Medical Experimental Animal Center (Foshan, Guangdong, China). Animals were

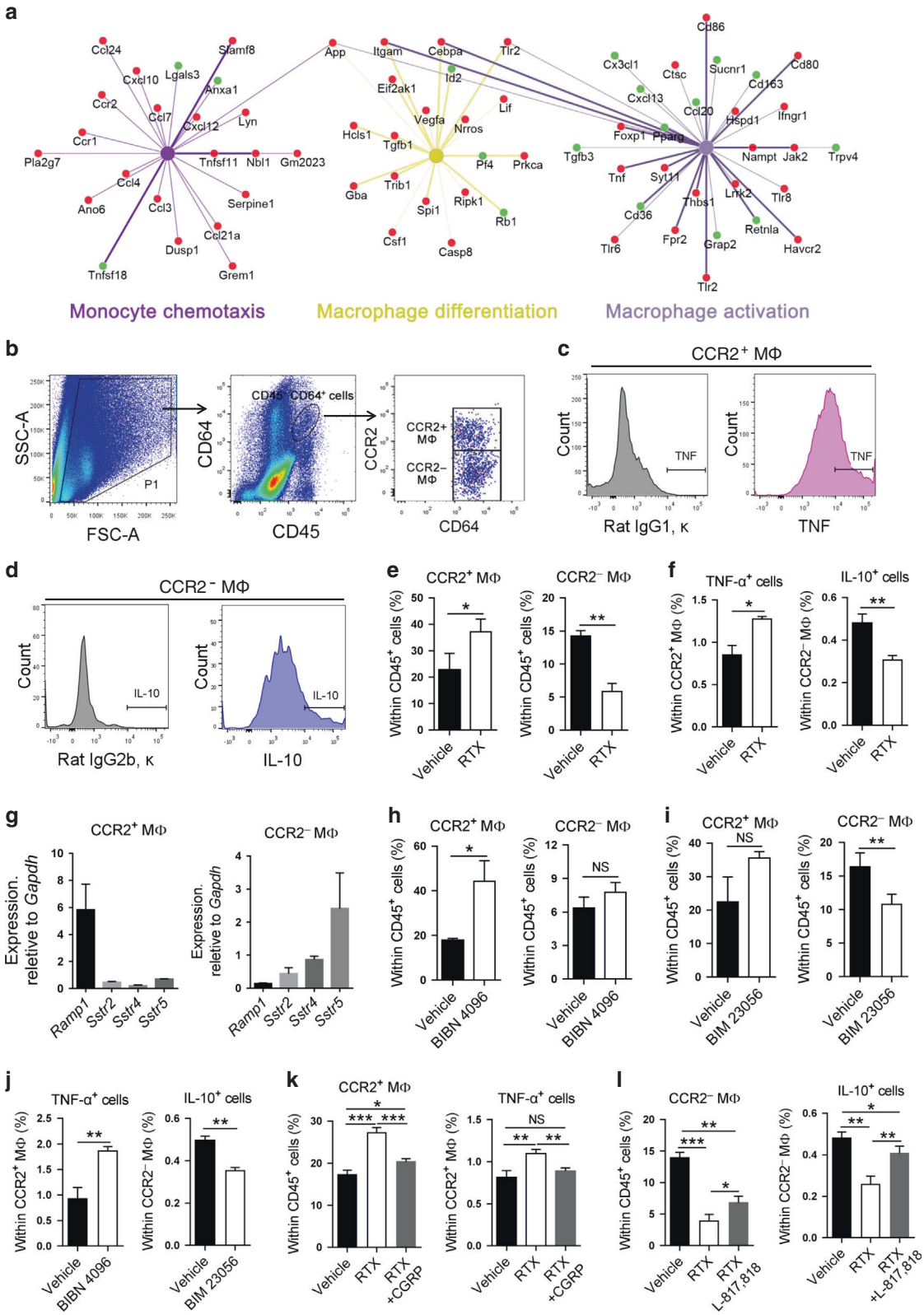


maintained in a 12 h light/12 h dark cycle and fed a standard laboratory diet and water *ad libitum*. All animal protocols in this study were approved by the Jinan University Laboratory Animal Committee on Animal Welfare. All animals were treated in accordance with the Association for Research in Vision and Ophthalmology Statement for the Use of Animals in Ophthalmic and Vision Research. The animals were anesthetized via inhalation of 2% isoflurane and euthanized using an overdose of $CO_2$ and cervical dislocation.

### Depletion of TRPV1$^+$ sensory nerves

RTX, a specific high-affinity agonist of TRPV1, was used to deplete TRPV1$^+$ sensory nerves as described previously[35,36]. Female C57BL/6 mice aged

**Fig. 6 Effect of TRPV1$^+$ sensory nerves on the responses of corneal macrophages. a** Cytoscape network analysis of transcripts involved in monocyte chemotaxis, macrophage differentiation, and macrophage activation (up-regulated genes are shown in red and down-regulated genes are shown in green). **b**–**d** The gating strategies of flow cytometry for analyzing the number of corneal CCR2$^+$ and CCR2$^-$ macrophages (**b**), production of TNF-α in CCR2$^+$ macrophages (**c**), and production of IL-10 in CCR2$^-$ macrophages (**d**). **e** Comparison of the number of CCR2$^+$ and CCR2$^-$ macrophages in the cornea between vehicle-treated mice and resiniferatoxin (RTX)-treated mice ($n = 3$ independent experiments, 5 mice per experiment in each group). **f** Changes in the production of TNF-α in CCR2$^+$ macrophages and IL-10 in CCR2$^-$ macrophages after RTX treatment ($n = 3$ independent experiments, 8 mice per experiment in each group). **g** Quantitative polymerase chain reaction (qPCR) analysis of *Ramp1* and *Sstr1–5* in corneal CCR2$^+$ and CCR2$^-$ macrophages ($n = 3$ independent experiments, 5 mice per experiment in each group). **h**, **i** Alteration in the number of CCR2$^+$ and CCR2$^-$ macrophages in the cornea after treatment with BIBN 4096 (**h**, $n = 3$ independent experiments, 5 mice per experiment in each group) or BIM 23056 (**i**, $n = 3$ independent experiments, 5 mice per experiment in each group). **j** Changes in the production of TNF-α in CCR2$^+$ macrophages after BIBN 4096 treatment and IL-10 in CCR2$^-$ macrophages after BIM 23056 treatment ($n = 3$ independent experiments, 8 mice per experiment in each group). **k** Difference in the number of CCR2$^+$ macrophages (*left*, $n = 3$ independent experiments, 5 mice per experiment in each group) and production of TNF-α in CCR2$^+$ macrophages (*right*, $n = 3$ independent experiments, 8 mice per experiment in each group) among vehicle-treated mice, RTX-treated mice, and RTX-treated mice following calcitonin gene-related peptide (CGRP) treatment. **l** Difference in the number of CCR2$^-$ macrophages (*left*, $n = 3$ independent experiments, 5 mice per experiment in each group) and production of IL-10 in CCR2$^-$macrophages (*right*, $n = 3$ independent experiments, 8 mice per experiment in each group) among vehicle-treated mice, RTX-treated mice, and RTX-treated mice following L-817,818 treatment. Data are presented as mean ± SD. $^*P < 0.05$, $^{**}P < 0.01$, and $^{***}P < 0.001$.

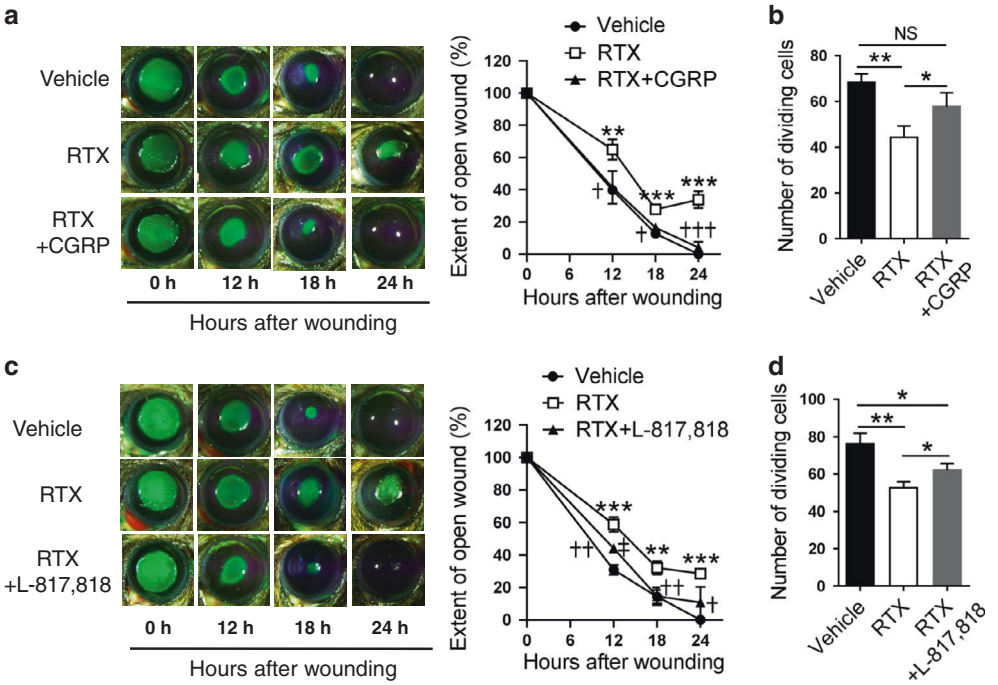


**Fig. 7 Effect of calcitonin gene-related peptide (CGRP) or L-817,818 on corneal wound healing in resiniferatoxin (RTX)-treated mice. a**, **c** Effect of CGRP or L-817,818 on wound closure in resiniferatoxin (RTX)-treated mice after epithelial abrasion. Images on the left show staining of the wounded corneal area at each time point after epithelial abrasion with fluorescein sodium. The graphs on the right show the dynamic changes in the ratio of wounded area within the whole corneal area from vehicle-treated mice, RTX-treated mice, and RTX-treated mice administered CGRP (**a**, $n = 6$ mice per group) or L-817,818 (**c**, $n = 6$ mice per group). **b**, **d** Comparison of the number of dividing epithelial cells among vehicle-treated mice, RTX-treated mice, and RTX-treated mice administered CGRP at 18 h after epithelial abrasion (**b**, $n = 6$ mice per group) or L-817,818 (**d**, $n = 6$ mice per group). Data are presented as mean ± SD. *RTX-treated mice vs. vehicle-treated mice, $^{\dagger}$RTX-treated mice with CGRP or L-817,818 treatment vs. RTX-treated mice, $^{\ddagger}$RTX-treated mice with L-817,818 treatment vs. vehicle-treated mice, $^{*,\dagger,\ddagger}P < 0.05$, $^{**,\dagger\dagger}P < 0.01$ and $^{***,\dagger\dagger\dagger}P < 0.001$.

four weeks were subcutaneously injected thrice with RTX (Tocris Bioscience, USA; no. 1137), and the dosage was increased over three consecutive days (30 μg/kg, 70 μg/kg, 100 μg/kg). To evaluate the effect of sensory nerve depletion, TRPV1 expression, corneal nerve density and sensitivity were measured 4 weeks after RTX treatment.

## Corneal nerve imaging and density measurement

Corneal nerve imaging and density measurement were performed as described previously[9,82,83]. Briefly, the cornea with complete limbus was in situ removed from euthanized animals, fixed in 2% formaldehyde, washed with phosphate buffered saline (PBS), permeabilized with 0.1% Triton X-100, blocked in 2% bovine serum albumin (BSA) in PBS, and incubated with neuron-specific beta-III tubulin Alexa Fluor 488-conjugated antibody (Sigma-Aldrich, USA; no. AB15708A4). Images of each corneal zone were captured using a DeltaVision Elite high-resolution microscope imaging system (GE Healthcare, USA) under a 40× objective. The length of the corneal nerve fibers was analyzed using the Imaris software (Bitplane, Switzerland). Briefly, the image of corneal nerve fibers was loaded into the Imaris software. β-III-tubulin-positive nerve fibers were detected, and their total length was calculated automatically. The nerve branch number or nerve length within 40× objective field of view of each corneal zone were represented as the relative nerve density of the specified corneal region.

## Measurement of corneal sensitivity

Corneal sensitivity was analyzed using a Cochet-Bonnet esthesiometer (Luneau SAS, France; no. 8630-1490-29), as published previously[83,84]. Briefly, at different time points after epithelial abrasion, unanesthetized mice were held by the scruff of the neck and presented with a

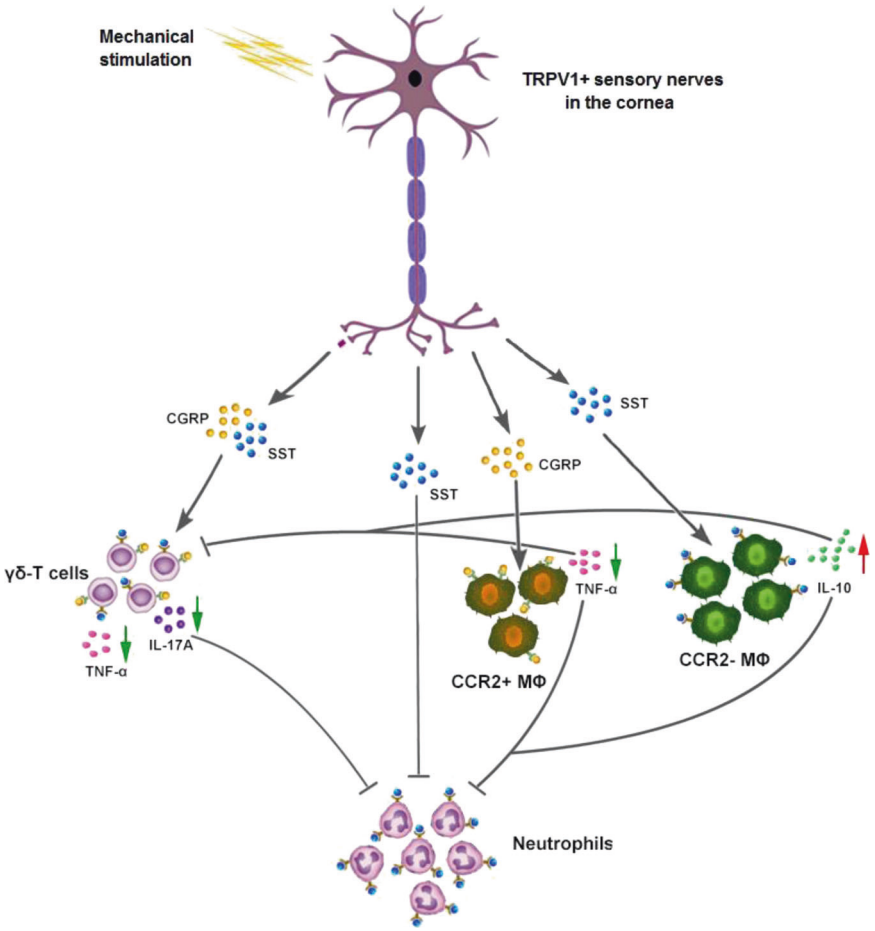


**Fig. 8 Model showing how TRPV1$^+$ sensory nerves modulate corneal inflammation after corneal injury.** Based on this study and other data, we hypothesize that corneal abrasions activate TRPV1$^+$ sensory nerve endings in the cornea to release the neuropeptides SST and CGRP, which reduce the degree of inflammatory response to corneal injury by binding to corresponding receptors expressed in different preferential ways on each of the three immune cell types. For neutrophils, the SST released from TRPV1$^+$ nerve terminals acts directly on neutrophils via the SST-SSTR5 axis to inhibit their recruitment to the injured cornea. As for γδ T cells, both the CGRP and SST released from TRPV1$^+$ nerve endings inhibited their infiltration and expression of the pro-inflammatory cytokines TNF-α and IL-17A via both the CGRP-RAMP1 and SST-SSTR5 pathways, thereby indirectly dampening neutrophil recruitment. Notably, for the two different macrophage populations in the cornea, TRPV1$^+$ sensory nerves then regulate the local inflammatory response through two different mechanisms. In the case of CCR2$^+$ macrophages, the CGRP from the nerve terminal inhibits their accumulation in the wounded cornea and production of the pro-inflammatory cytokine TNF-α by binding to the corresponding receptor RAMP1 on the macrophages. However, for CCR2$^-$ macrophages, the SST released from nerve terminals promotes their recruitment to the injured cornea and production of the immunosuppressive cytokine IL-10 by binding to the macrophage-expressed receptor SSTR5. Ultimately, TRPV1 + sensory nerves control the inflammatory response process after corneal trauma to an appropriate level through the direct and indirect action of released neuropeptides on different immune cells and the interaction between different immune cells.

monofilament at lengths ranging from 6.0 to 0.5 cm in 0.5 cm increments to elicit a blink response. At each length, the monofilament touched the cornea four times, making perpendicular contact with the surface before considering a response to be negative (no blink response). The lack of a blink reflex at a monofilament length of 0.5 cm was recorded as "0." All the measurements were performed by the same examiner, who was blinded to the animal groups.

## Corneal wound healing model

Mouse corneas were mechanically abraded as described previously[8–13]. Briefly, the animals were anesthetized using an intraperitoneal injection of sodium phenobarbital (25–50 mg/kg). The central corneal epithelium was marked with a 2 mm trephine, and this labeled region was removed using a golf club spud (Accutome, Malvern, PA, USA).

## Pharmacological agonism and antagonism

AMG-517 was used to block the function of TRPV1. Mouse eyes were pretreated for three days with AMG-517 (3 µl, 1 µg/µl; Selleck, USA; no. 659730-32-2) (three times each day) before corneal epithelial abrasion. Subsequently, the same concentration of AMG-517 was administered to the eyes after corneal epithelial abrasion every 6 h. To determine the roles of the CGRP receptor (RAMP1) and SSTR5 in modulating the recruitment of neutrophils and γδ T cells, as well as the responses of corneal CCR2$^-$ and CCR2$^+$ macrophages, CGRP (3 µl, 0.5 µg/µl; R&D Systems; no. 1161) or the agonist of SSTR5, L-817,818 (3 µl, 0.25 µg/µl; R&D Systems; no. 1980), was administered to the eyes of RTX-treated mice at −6, 0, 6, 12, 18, and 24 h after corneal epithelial abrasion. The antagonist of RAMP1, BIBN 4096 (3 µl, 2 µg/µl; Tocris Bioscience, USA; no. 4561), or the antagonist of SSTR5, BIM 23056 (3 µl, 2 µg/µl; R&D Systems; no. 1844), was administered to the eyes of normal mice at −6, 0, 6, 12, 18, and 24 h after corneal epithelial abrasion.

## Immunostaining

The procedure was performed as described previously[8–13]. In brief, mouse eyes were fixed in 2% formaldehyde solution for one hour and dissected with corneal scissors under the dissecting microscope to obtain corneas with complete limbi. Corneas were washed thrice in PBS, blocked in 2% BSA for 15 min, and permeabilized in 0.1% Triton-X 100 for 15 min. Next, corneal tissues were incubated overnight with anti-β-III tubulin antibody conjugated with Alexa Fluor 488 (1:100; Sigma-Aldrich; no. AB15708A4),

**Table 1.** PCR primers used in this study.

| Gene Name | | Primer Sequence |
|---|---|---|
| *Cgrp* | Forward | 5′-CAACAAGTTTCACACCTTCC-3′ |
| | Reverse | 5′-ATTCTCTTTTAGCCTGTGGG-3′ |
| *Sst* | Forward | 5′-CCCAACCAGACAGAGAATGA-3′ |
| | Reverse | 5′-AGGAAGAGATATGGGGTTTG-3′ |
| *Ramp1* | Forward | 5′-GACCATACAAGTTTGCAGGA-3′ |
| | Reverse | 5′-CCAACGAGATTCTGTGATGA-3′ |
| *Sstr1* | Forward | 5′-AAATCTCCAGGTACAGGTTTA-3′ |
| | Reverse | 5′-CATTAAGTGGAAAGGCTCTGG-3′ |
| *Sstr2* | Forward | 5′-CTAAATCAAAGTCCTGTGTGT-3′ |
| | Reverse | 5′-CTTTTCTTCAGGTTCAGCGT-3′ |
| *Sstr3* | Forward | 5′-TTGCTCATTGTGGTAAAGGT-3′ |
| | Reverse | 5 ′-TGACGATGTTGAGCAGATAG-3′ |
| *Sstr4* | Forward | 5′-CCATCGGATTATGCTACCTG-3′ |
| | Reverse | 5 -CATAGAGAATGGGATTGGCA-3′ |
| *Sstr5* | Forward | 5′-GCTCATGTCTCTGCCGCTCTTG-3′ |
| | Reverse | 5′-GCAGCCTTCACCTTCACTACGATG-3′ |
| *Il1β* | Forward | 5′-TTTGAAGTTGACGGACCCCAA-3′ |
| | Reverse | 5′-TCATATGGGTCCGACAGCAC-3′ |
| *Il18* | Forward | 5′-ACACGCTTTACTTTATACCTG-3′ |
| | Reverse | 5′-ACTTGGTCATTTATATTCCGTA-3′ |
| *Il17a* | Forward | 5′-ATCTGTGTCTCTGATGCTGTTG-3′ |
| | Reverse | 5′-GGAACGGTTGAGGTAGTCTGA-3′ |
| *Tnfa* | Forward | 5′-CATCTCCCTCCAGAAAAGAC-3′ |
| | Reverse | 5′-AGAAGATGATCTGAGTGTGAG-3′ |
| *Gapdh* | Forward | 5′-CAAGGACACTGAGCAAGAG-3′ |
| | Reverse | 5′-TGCAGCGAACTTTATTGATG-3′ |

anti-mouse TRPV1 antibody (1:100; ABclonal; no. A8564), anti-mouse CGRP antibody (1:100; ABclonal; no. A5542), anti-mouse SST antibody (1:100; ABclonal; no. A20617), anti-mouse Ly6G antibody conjugated with fluorescein isothiocyanate (FITC) (1:100; BD Biosciences, USA; no. 551460), or anti-mouse GL3 antibody conjugated with phycoerythrin (PE) (1:100; BD Biosciences; no. 553178) at 4 °C. Corneas incubated with anti-TRPV1/CGRP/SST antibodies were washed three times with PBS and then incubated with Alexa Fluor 594-conjugated secondary antibody anti-rabbit IgG (1:100; ABclonal; No. AS039) at 4 °C overnight. Then, the corneas were washed thrice in PBS, placed on a glass slide, and cut radially in four directions with surgical blades while flattening them. A fluorescent mounting medium containing 1 μM 4′,6-diamidino-2-phenylindole (DAPI) (Sigma-Aldrich, USA; no. 28718-90-3) was placed on the corneas. Images of the corneas were analyzed using the DeltaVision microscopy imaging system (Applied Precision, Issaquah, WA, USA).

## RNA sequencing

RNA sequencing from corneal bulk RNA was carried out as previously described[85,86]. In brief, total corneal RNA purity and concentration were determined. After RNA integrity was verified, construction and sequencing of the cDNA library were performed by the Beijing Genomics Institute (BGI) using the BGISEQ-500 platform. Each sample produced more than 20 M clean reads, which were mapped to the mm10 reference genome version using Spliced Transcripts Alignment to a Reference (STAR2.5.3a).

## Flow cytometric analysis

Corneas with complete limbi were cut into pieces and digested in 4 mg/ml collagenase I (Sigma-Aldrich, no. C0130) for 30 min. The digested suspension of corneal tissues was washed twice in PBS and passed through a 75 μm filter to obtain single cells. Then, corneal cells were blocked using flow cytometry staining buffer (eBioscience, USA; no. 00-4222-57) containing anti-mouse CD16/32 antibody at room temperature for 10 min. To analyze neutrophils and γδ T cells, corneal cells were incubated with the following antibodies (1:100): anti-mouse CD45 antibody conjugated with allophycocyanin (APC) (BD Biosciences; no. 559864), anti-mouse CD11b antibody conjugated with Percp Cy5.5 (BD Biosciences; no. 550993), anti-mouse Ly6G antibody conjugated with FITC (BD Biosciences; no. 551460), and anti-mouse GL3 antibody conjugated with PE (BD Biosciences; no. 553178) at room temperature for 30 min. To analyze macrophages, corneal cells were incubated with the following antibodies (1:100): anti-mouse CD45 antibody conjugated with FITC (BD Biosciences; no. 553080), anti-mouse CD64 antibody conjugated with Brilliant violet 421 (Biolegend, USA; no. 139309), and anti-mouse CCR2 antibody conjugated with PE (R&D Systems; no. FAB5538P) at room temperature for 30 min. To detect the production of TNF-α and IL-10 by the macrophages, the above stained corneal cells were fixed in 4% paraformaldehyde for 40 min and permeabilized in 0.01% Triton X-100 for 8 min. These cells were washed in PBS and incubated with anti-mouse TNF-α antibody conjugated with APC (1:100; Biolegend; no. 506308) or IL-10 antibody conjugated with APC (1:100; Biolegend; no. 505010) at room temperature for 30 min. Finally, these stained corneal cells were analyzed using BD FACSCanto.

## Transcript amplification from neutrophils, γδ T cells, and corneal macrophages

Single corneal cells were incubated with the following antibodies: anti-mouse CD45 antibody conjugated with APC, anti-mouse CD11b antibody conjugated with Percp Cy5.5, anti-mouse Ly6G antibody conjugated with FITC, and anti-mouse GL3 antibody conjugated with PE, or anti-mouse CD45 antibody conjugated with FITC, anti-mouse CD64 antibody conjugated with Brilliant violet 421, and anti-mouse CCR2 antibody conjugated with PE at room temperature for 30 min. After washing with PBS, these cells were analyzed using the BD FACSAria to obtain $CD45^+CD11b^+Ly6G^+$ neutrophils, $CD45^+CD11b^-GL3^+$ γδ T cells, and $CD45^+CD64^+CCR2^-$ and $CD45^+CD64^+CCR2^+$ macrophages. The mRNA of the sorted neutrophils, γδ T cells, and $CCR2^-$ or $CCR2^+$ macrophages was amplified and converted into DNA using a REPLI-gWTA single cell kit (Qiagen, no. 150063).

## qPCR

Corneas with complete limbi were placed in buffer RZ (Tiangen; no. RK145) and smashed using a TissueRuptor (Qiagen, Germantown, MD). The total RNA of corneal tissues was extracted using the RNAsimple total RNA kit (Tiangen; no. DP419). cDNA was obtained from total RNA of corneal tissues using a ReverTra Ace qPCR RT kit (Toyobo, Japan; no. FSQ-101). The expression of target genes in corneal cDNA or amplified DNA of neutrophils, γδ T cells, and macrophages were analyzed using the THUNDERBIRD SYBR qPCR mix (Toyobo; no. QPS-201). The primers used in this study are shown in the Table 1.

## Statistical analysis

Data are presented as mean ± standard deviation (SD). For comparisons between groups, one-way analysis of variance was performed. Statistical significance was set at $P < 0.05$.

## REFERENCES

1. Ljubimov, A. V. & Saghizadeh, M. Progress in corneal wound healing. *Prog. Retin. Eye Res.* **49**, 17–45 (2015).
2. Medeiros, C. S. & Santhiago, M. R. Corneal nerves anatomy, function, injury and regeneration. *Exp. Eye Res.* **200**, 108243 (2020).
3. McGwin, G. Jr & Owsley, C. Incidence of emergency department-treated eye injury in the United States. *Arch. Ophthalmol.* **123**, 662–666 (2005).
4. Bizrah, M., Yusuf, A. & Ahmad, S. An update on chemical eye burns. *Eye (Lond.)* **33**, 1362–1377 (2019).
5. Netto, M. V. et al. Wound healing in the cornea: A review of refractive surgery complications and new prospects for therapy. *Cornea* **24**, 509–522 (2005).
6. Spadea, L., Giammaria, D. & Trabucco, P. Corneal wound healing after laser vision correction. *Br. J. Ophthalmol.* **100**, 28–33 (2016).
7. Saghizadeh, M., Kramerov, A. A., Svendsen, C. N. & Ljubimov, A. V. Concise Review: Stem Cells for Corneal Wound Healing. *Stem Cells* **35**, 2105–2114 (2017).
8. Li, Z., Burns, A. R. & Smith, C. W. Two waves of neutrophil emigration in response to corneal epithelial abrasion: distinct adhesion molecule requirements. *Invest Ophthalmol. Vis. Sci.* **47**, 1947–1955 (2006).

9. Li, Z., Burns, A. R., Han, L., Rumbaut, R. E. & Smith, C. W. IL-17 and VEGF are necessary for efficient corneal nerve regeneration. *Am. J. Pathol.* **178**, 1106–1116 (2011).
10. Li, Z., Burns, A. R. & Smith, C. W. Lymphocyte function-associated antigen-1-dependent inhibition of corneal wound healing. *Am. J. Pathol.* **169**, 1590–1600 (2006).
11. Liu, Q., Smith, C. W., Zhang, W., Burns, A. R. & Li, Z. NK cells modulate the inflammatory response to corneal epithelial abrasion and thereby support wound healing. *Am. J. Pathol.* **181**, 452–462 (2012).
12. Liu, J. et al. CCR2(−) and CCR2(+) corneal macrophages exhibit distinct characteristics and balance inflammatory responses after epithelial abrasion. *Mucosal Immunol.* **10**, 1145–1159 (2017).
13. Li, F., Yu, R., Sun, X., Chen, X., Xu, P., Huang, Y. et al. Autonomic nervous system receptor-mediated regulation of mast cell degranulation modulates the inflammation after corneal epithelial abrasion. *Exp. Eye. Res.* **219**, 109065 (2022).
14. Li, Z., Burns, A. R., Miller, S. B. & Smith, C. W. CCL20, γδ T cells, and IL-22 in corneal epithelial healing. *FASEB J.* **25**, 2659–2668 (2011).
15. Liu, J. et al. Local Group 2 Innate Lymphoid Cells Promote Corneal Regeneration after Epithelial Abrasion. *Am. J. Pathol.* **187**, 1313–1326 (2017).
16. Belmonte, C., Acosta, M. C. & Gallar, J. Neural basis of sensation in intact and injured corneas. *Exp. Eye Res.* **78**, 513–525 (2004).
17. Belmonte, C., Aracil, A., Acosta, M. C., Luna, C. & Gallar, J. Nerves and sensations from the eye surface. *Ocul. Surf.* **2**, 248–253 (2004).
18. Belmonte, C. et al. TFOS DEWS II pain and sensation report. *Ocul. Surf.* **15**, 404–437 (2017).
19. Parra, A. et al. Ocular surface wetness is regulated by TRPM8-dependent cold thermoreceptors of the cornea. *Nat. Med.* **16**, 1396–1399 (2010).
20. Alamri, A., Bron, R., Brock, J. A. & Ivanusic, J. J. Transient receptor potential cation channel subfamily V member 1 expressing corneal sensory neurons can be subdivided into at least three subpopulations. *Front. Neuroanat.* **9**, 71 (2015).
21. Chu, C., Artis, D. & Chiu, I. M. Neuro-immune Interactions in the Tissues. *Immunity* **52**, 464–474 (2020).
22. Baral, P., Udit, S. & Chiu, I. M. Pain and immunity: implications for host defence. *Nat. Rev. Immunol.* **19**, 433–447 (2019).
23. Pinho-Ribeiro F. A., Verri W. A., Jr. & Chiu I. M. Nociceptor sensory neuron-immune interactions in pain and inflammation. *Trends Immunol.* 38, 5–19 (2017).
24. Cohen, J. A., Wu, J. & Kaplan, D. H. Neuronal regulation of cutaneous immunity. *J. Immunol.* **204**, 264–270 (2020).
25. Baral, P. et al. Nociceptor sensory neurons suppress neutrophil and gammadelta T cell responses in bacterial lung infections and lethal pneumonia. *Nat. Med.* **24**, 417–426 (2018).
26. Baliu-Pique, M., Jusek, G. & Holzmann, B. Neuroimmunological communication via CGRP promotes the development of a regulatory phenotype in TLR4-stimulated macrophages. *Eur. J. Immunol.* **44**, 3708–3716 (2014).
27. Gomes, R. N. et al. Calcitonin gene-related peptide inhibits local acute inflammation and protects mice against lethal endotoxemia. *Shock* **24**, 590–594 (2005).
28. Williams, R., Zou, X. & Hoyle, G. W. Tachykinin-1 receptor stimulates proinflammatory gene expression in lung epithelial cells through activation of NF-kappaB via a G(q)-dependent pathway. *Am. J. Physiol. Lung Cell Mol. Physiol.* **292**, L430–L437 (2007).
29. Helyes, Z. et al. Antiinflammatory and analgesic effects of somatostatin released from capsaicin-sensitive sensory nerve terminals in a Freund's adjuvant-induced chronic arthritis model in the rat. *Arthritis Rheum.* **50**, 1677–1685 (2004).
30. Helyes, Z. et al. Role of transient receptor potential vanilloid 1 receptors in endotoxin-induced airway inflammation in the mouse. *Am. J. Physiol. Lung Cell Mol. Physiol.* **292**, L1173–L1181 (2007).
31. Lin, T. et al. Pseudomonas aeruginosa-induced nociceptor activation increases susceptibility to infection. *PLoS Pathog.* **17**, e1009557 (2021).
32. Yuan, K. et al. Sensory nerves promote corneal inflammation resolution via CGRP mediated transformation of macrophages to the M2 phenotype through the PI3K/AKT signaling pathway. *Int. Immunopharmacol.* **102**, 108426 (2022).
33. Zhang, Y. et al. Role of VIP and sonic Hedgehog signaling pathways in mediating epithelial wound healing, sensory nerve regeneration, and their defects in diabetic corneas. *Diabetes* **69**, 1549–1561 (2020).
34. Sumioka, T. et al. Impairment of corneal epithelial wound healing in a TRPV1-deficient mouse. *Invest Ophthalmol. Vis. Sci.* **55**, 3295–3302 (2014).
35. Baral, P. et al. Nociceptor sensory neurons suppress neutrophil and γδ T cell responses in bacterial lung infections and lethal pneumonia. *Nat. Med.* **24**, 417–426 (2018).
36. Mishra S. K. & Hoon M. A. Ablation of TrpV1 neurons reveals their selective role in thermal pain sensation. *Mol. Cell. Neurosci.* **43**, 157–163 (2010).
37. Bai, J., Liu, F., Wu, L. F., Wang, Y. F. & Li, X. Q. Attenuation of TRPV1 by AMG-517 after nerve injury promotes peripheral axonal regeneration in rats. *Mol. Pain.* **14**, 1744806918777614 (2018).
38. Gavva, N. R. et al. Pharmacological blockade of the vanilloid receptor TRPV1 elicits marked hyperthermia in humans. *Pain* **136**, 202–210 (2008).
39. Jung, H., Yoon, B. C. & Holt, C. E. Axonal mRNA localization and local protein synthesis in nervous system assembly, maintenance and repair. *Nat. Rev. Neurosci.* **13**, 308–324 (2012).
40. Glock, C., Heumuller, M. & Schuman, E. M. mRNA transport & local translation in neurons. *Curr. Opin. Neurobiol.* **45**, 169–177 (2017).
41. Holzmann, B. Modulation of immune responses by the neuropeptide CGRP. *Amino Acids* **45**, 1–7 (2013).
42. Fernandes, E. S. et al. TRPV1 deletion enhances local inflammation and accelerates the onset of systemic inflammatory response syndrome. *J. Immunol.* **188**, 5741–5751 (2012).
43. Lu, S., Li, D., Xi, L. & Calderone, R. Interplay of interferon-gamma and macrophage polarization during Talaromyces marneffei infection. *Micro. Pathog.* **134**, 103594 (2019).
44. Galarraga-Vinueza, M. E. et al. Macrophage polarization in peri-implantitis lesions. *Clin. Oral. Investig.* **25**, 2335–2344 (2021).
45. Funes, S. C., Rios, M., Escobar-Vera, J. & Kalergis, A. M. Implications of macrophage polarization in autoimmunity. *Immunology* **154**, 186–195 (2018).
46. Zhao, S. et al. Tumor-derived exosomal miR-934 induces macrophage M2 polarization to promote liver metastasis of colorectal cancer. *J. Hematol. Oncol.* **13**, 156 (2020).
47. Quero, L. et al. miR-221-3p Drives the Shift of M2-Macrophages to a pro-inflammatory function by suppressing JAK3/STAT3 activation. *Front Immunol.* **10**, 3087 (2019).
48. Keiran, N. et al. SUCNR1 controls an anti-inflammatory program in macrophages to regulate the metabolic response to obesity. *Nat. Immunol.* **20**, 581–592 (2019).
49. Chiu, I. M. et al. Bacteria activate sensory neurons that modulate pain and inflammation. *Nature* **501**, 52–57 (2013).
50. Wang, J. Neutrophils in tissue injury and repair. *Cell Tissue Res.* **371**, 531–539 (2018).
51. Zhu, S. N. & Dana, M. R. Expression of cell adhesion molecules on limbal and neovascular endothelium in corneal inflammatory neovascularization. *Invest Ophthalmol. Vis. Sci.* **40**, 1427–1434 (1999).
52. Kolaczkowska, E. & Kubes, P. Neutrophil recruitment and function in health and inflammation. *Nat. Rev. Immunol.* **13**, 159–175 (2013).
53. Trankner, D., Hahne, N., Sugino, K., Hoon, M. A. & Zuker, C. Population of sensory neurons essential for asthmatic hyperreactivity of inflamed airways. *Proc. Natl Acad. Sci. USA* **111**, 11515–11520 (2014).
54. Cohen, J. A. et al. Cutaneous TRPV1(+) neurons trigger protective innate type 17 anticipatory immunity. *Cell* **178**, 919–932 e914 (2019).
55. Gonzalez-Gonzalez, O., Bech, F., Gallar, J., Merayo-Lloves, J. & Belmonte, C. Functional properties of sensory nerve terminals of the mouse cornea. *Invest Ophthalmol. Vis. Sci.* **58**, 404–415 (2017).
56. Hadrian, K. et al. Macrophage-mediated tissue vascularization: Similarities and differences between cornea and skin. *Front. Immunol.* **12**, 667830 (2021).
57. Bukowiecki A., Hos D., Cursiefen C. & Eming S. A. Wound-healing studies in cornea and skin: Parallels, Differences and Opportunities. *Int. J. Mol. Sci.***18**, 1257 (2017).
58. Lowes, M. A., Russell, C. B., Martin, D. A., Towne, J. E. & Krueger, J. G. The IL-23/T17 pathogenic axis in psoriasis is amplified by keratinocyte responses. *Trends Immunol.* **34**, 174–181 (2013).
59. Riol-Blanco, L. et al. Nociceptive sensory neurons drive interleukin-23-mediated psoriasiform skin inflammation. *Nature* **510**, 157–161 (2014).
60. Kashem, S. W. et al. Nociceptive sensory fibers drive Interleukin-23 production from CD301b+ dermal dendritic cells and drive protective cutaneous immunity. *Immunity* **43**, 515–526 (2015).
61. Liu, J. & Li, Z. Resident innate immune cells in the cornea. *Front. Immunol.* **12**, 620284 (2021).
62. Li, Z., Burns, A. R., Rumbaut, R. E. & Smith, C. W. gamma delta T cells are necessary for platelet and neutrophil accumulation in limbal vessels and efficient epithelial repair after corneal abrasion. *Am. J. Pathol.* **171**, 838–845 (2007).
63. Xue, Y. et al. The mouse autonomic nervous system modulates inflammation and epithelial renewal after corneal abrasion through the activation of distinct local macrophages. *Mucosal Immunol.* **11**, 1496–1511 (2018).
64. Chen, O., Donnelly, C. R. & Ji, R. R. Regulation of pain by neuro-immune interactions between macrophages and nociceptor sensory neurons. *Curr. Opin. Neurobiol.* **62**, 17–25 (**2020**).
65. Muschter D., et al. Sensory neuropeptides and their receptors participate in mechano-regulation of murine macrophages. *Int. J. Mol. Sci.* **20**, 503 (2019).
66. Baliu-Pique M., Jusek G. Fau - Holzmann B. & Holzmann B. Neuroimmunological communication via CGRP promotes the development of a regulatory phenotype in TLR4-stimulated macrophages. *Eur. J. Immunol.* **44**, 3708–3716 (2014).
67. Russell F. A., King R., Smillie S. J., Kodji X. & Brain S. D. Calcitonin gene-related peptide: physiology and pathophysiology. *Physiol Rev*. **94**, 1099–1142 (2014).
68. Harzenetter M. D., et al. Negative regulation of TLR responses by the neuropeptide CGRP is mediated by the transcriptional repressor ICER. *J Immunol*. **179**, 607–615 (2007).

69. Gomes R. N., et al. Calcitonin gene-related peptide inhibits local acute inflammation and protects mice against lethal endotoxemia. *Shock*. **24**, 590–594 (2005).
70. Martínez, C. et al. Vasoactive intestinal peptide and pituitary adenylate cyclase-activating polypeptide modulate endotoxin-induced IL-6 production by murine peritoneal macrophages. *J. Leukoc. Biol.* **63**, 591–601 (1998).
71. Delgado, M. et al. Vasoactive intestinal peptide and pituitary adenylate cyclase-activating polypeptide inhibit tumor necrosis factor α transcriptional activation by regulating nuclear factor-kB and cAMP response element-binding protein/c-Jun. *J. Biol. Chem.* **273**, 31427–31436 (1998).
72. Hoeffel, G. et al. Sensory neuron-derived TAFA4 promotes macrophage tissue repair functions. *Nature* **594**, 94–99 (2021).
73. Gao, N., Yin, J., Yoon, G. S., Mi, Q. S. & Yu, F. S. Dendritic cell-epithelium interplay is a determinant factor for corneal epithelial wound repair. *Am. J. Pathol.* **179**, 2243–2253 (2011).
74. Gao, Y. et al. NK cells are necessary for recovery of corneal CD11c+ dendritic cells after epithelial abrasion injury. *J. Leukoc. Biol.* **94**, 343–351 (2013).
75. Liu, J. et al. Mast cells participate in corneal development in mice. *Sci. Rep.* **5**, 17569 (2015).
76. Sahu, S. K. et al. Mast cells initiate the recruitment of neutrophils following ocular surface injury. *Invest Ophthalmol. Vis. Sci.* **59**, 1732–1740 (2018).
77. Elbasiony E., Mittal S. K., Foulsham W., Cho W. & Chauhan S. K. Epithelium-derived IL-33 activates mast cells to initiate neutrophil recruitment following corneal injury. *Ocul Surf.* **18**, 633–640 (2020).
78. Perner, C. et al. Substance P release by sensory neurons triggers dendritic cell migration and initiates the Type-2 immune response to allergens. *Immunity* **53**, 1063–1077 (2020).
79. Nussbaum, J. C. et al. Type 2 innate lymphoid cells control eosinophil homeostasis. *Nature* **502**, 245–248 (2013).
80. Talbot, S. et al. Silencing Nociceptor. *Neurons Reduces Allerg. Airw. Inflamm. Neuron* **87**, 341–354 (2015).
81. Blake, K. J., Jiang, X. R. & Chiu, I. M. Neuronal Regulation of Immunity in the Skin and Lungs. *Trends Neurosci.* **42**, 537–551 (2019).
82. Liu, J. et al. Antibiotic-induced dysbiosis of gut microbiota impairs corneal nerve regeneration by affecting CCR2-negative macrophage distribution. *Am. J. Pathol.* **188**, 2786–2799 (2018).
83. Wang, H. et al. Epothilone B speeds corneal nerve regrowth and functional recovery through microtubule stabilization and increased nerve beading. *Sci. Rep.* **8**, 2647 (2018).
84. Chucair-Elliott, A. J., Zheng, M. & Carr, D. J. Degeneration and regeneration of corneal nerves in response to HSV-1 infection. *Invest Ophthalmol. Vis. Sci.* **56**, 1097–1107 (2015).
85. He, J. et al. Short-term high fructose intake impairs diurnal oscillations in the murine cornea. *Invest Ophthalmol. Vis. Sci.* **62**, 22 (2021).
86. Jiao, X., Wu, M., Lu, D., Gu, J. & Li, Z. Transcriptional profiling of daily patterns of mRNA expression in the C57BL/6J mouse cornea. *Curr. Eye Res.* **44**, 1054–1066 (2019).

## ACKNOWLEDGEMENTS

This work was supported by the National Natural Science Foundation of China through Grants 82171014 (to Z.L.), 32100715 (to J.L.), and 81770962 (to Z.L.), the Science and Technology Program of Guangzhou of China through Grant 202102020002 (to J.L.), and the PhD Start-up Fund of the Natural Science Foundation of Guangdong Province of China through Grant 2018A030310605 (to J.L.).

## AUTHOR CONTRIBUTIONS

Z.L. and J.L. conceived and designed the study. S.H. analyzed immunostaining and performed qPCR. R.Y., X.C., F.L., X.S., and P.X. helped with treatment of the animals, including the establishment of corneal injured model and drug treatment. J.L. performed flow cytometry analysis. Y.H., Y.X., and T.F. conducted the statistical analysis. J.L. drafted the first version of the paper. Z.L. critically reviewed and revised the paper for intellectual content. All authors critiqued the manuscript and approved its submission.

## COMPETING INTERESTS

The authors declare no competing interests.

## ADDITIONAL INFORMATION

**Supplementary information** The online version contains supplementary material available at https://doi.org/10.1038/s41385-022-00533-8.

**Correspondence** and requests for materials should be addressed to Zhijie Li.